Proceedings of the 17th World Congress
The International Federation of Automatic Control
Seoul, Korea, July 6-11, 2008

Tail-sitter UAV having one tilting rotor: Modeling, Control and Real-Time Experiments

O. Garcia, A. Sanchez, J. Escareño, R. Lozano

Université de Technologie de Compiègne, Heudiasyc UMR 6599,Centre de Recherches de Royallieu BP 20529, 60205 Compiègne Cedex, FRANCE (Tel: + 33 (0)3 44 23 44 23; e-mail: {ogarcias, asanchez, jescaren, rlozano}@hds.utc.fr).

Abstract: In this paper we address the development of a single-rotor tail-sitter Unmanned Aerial Vehicle (UAV), whose configuration provides structural benefits for flight stabilization. The mathematical model of the vertical take-off landing (VTOL) aircraft is obtained through the Newton-Euler approach. In order to stabilize the vehicle we employ a control algorithm based on separated saturation functions. To perform an on-board control, we have designed and manufactured a customized embedded system. The simulation and experimental results show the good performance of the aircraft in autonomous hover flight, even in the presence of external perturbations.

1. INTRODUCTION

Recently, mini Unmanned Aerial Vehicles or UAVs have became an interesting topic among scientific community due to the wide variety of applications, either military or civilian. Concerning the military applications, they can be highlighted the data collection of sensible areas (hostile zone, toxic environments, ports, and borders). For the civilian field an important application is natural disaster assessment(earthquakes, floods, and tornados), as well as search and rescue operations.

There exists a wide number of applications for mini UAVs, with great interest on reconnaissance and surveillance missions. Indeed, the nature of the mission to be accomplished defines the operational profile (design) of the UAV. This reveals the impact of vehicles that offers a wide operational scope to perform different kinds of missions. Operational flexibility is provided by convertible UAVs (CUAVs), since they blend the helicopter capabilities (vertical take-off/landing, hover) with airplane advantages (range, endurance). Naturally, the flight performance in both modalities decreases due to the structural trade-off in this type of vehicles.

Tail-sitter UAVs have a number of advantages compared to other configurations (Stone [2002]). In comparison to conventional designs they don't require a runway for launch and recovery because they possess much greater operational flexibility and can operate from any small clear space. While other conventional designs partially overcome this limitation via the use of takeoff and landing aids such as catapults and parachutes, these all entail extra system complexity and logistic support. Although helicopter UAVs share the same operational flexibility as the tail-sitter, they suffer from well-known deficiencies in terms of range, endurance and forward speed limitations due to the lower efficiency of rotor-born, rather than wing-born flight. Lastly, other configurations that have been developed to achieve the same goals as the tail-sitter, such as the tilt-wing, tilt-rotor and tilt-body, do so at the expense of significantly increased mechanical complexity compared to a tail-sitter that uses propeller wash over normal aircraft control surfaces to effect vertical flight control. By joining the takeoff and landing capabilities of the helicopter with the forward flight efficiencies of fixed-wing aircraft in such a simple way, the tail-sitter promises a unique blend of capabilities at lower cost than other UAV configurations.

During the hover-flight regime, most single-rotor aircrafts employ the propeller to provide thrust and air slipstream to control surfaces (elevator, ailerons, rudder), as a result, the dynamics stabilization is totally based on the aerodynamic torques. In the present paper we are interested in the stabilization of a single-rotor tail-sitter CUAV (see Fig. 1) at hover flight. The proposed configuration is based on a reduced mechanics, which simplifies its maintenance and replacement. In addition, we have incorporated certain structural features to improve the stability of the aircraft with respect to external perturbations. The operation description and dynamic model are presented in section 2. The control algorithm based on separated saturation

Fig. 1. Experimental prototype.

functions is described in section 3. In the section 4 we show the simulation results of full system and the section 5 shows the experimental results in real time of the vehicle. Conclusions are given in the section 6.

2. THE T-PLANE: A TAIL-SITTER TILTROTOR UAV

This section describes the operational description of the aircraft, and the structural advantages to improve the flight stability. Furthermore, the mathematical model of the vehicle is obtained using the rigid-body equations (Goldstein et al. [1983]).

2.1 Description

Our prototype reduces the aerodynamic dependence by incorporating a tilting rotor. This modification improves the robustness of the hover flight with respect to external perturbations. In order to control the roll motion, the aircraft tilts the propeller proportionally to the roll-angle feedback so that the vehicle can maintain the vertical position. This fact will provide a pendulum-like behavior, i.e. the propeller acts as the pendulum's screw while the fuselage represents the rod-bob. Furthermore, we introduce a transversal surface (see Fig. 2) in the same axis of the vertical air-slipstream vector, as a result, the surface will tend to remain inside of the air trajectory, damping the possible perturbations (mechanical gyro). The parallel deflection of the ailerons controls the pitch motion, while the differential deflection controls the yaw motion (see Fig. 3 and Fig. 4). The altitude of the T-Plane is driven by decreasing or increasing the propeller thrust.

2.2 Dynamic model

Let $\mathcal{I}$=$\{i_x^{\mathcal{I}}, j_y^{\mathcal{I}}, k_z^{\mathcal{I}}\}$ denote the righthanded inertial frame and $\mathcal{B}$=$\{i_x^{\mathcal{B}}, j_y^{\mathcal{B}}, k_z^{\mathcal{B}}\}$ denotes frame attached to the aircraft body whose origin is located at its center of gravity (see Fig. 2). The frame $\mathcal{R}$=$\{i_x^{\mathcal{R}}, j_y^{\mathcal{R}}, k_z^{\mathcal{R}}\}$ is considered during the tilting motion at regulating the roll motion.

Let the vector $\mathbf{q} = (\xi, \eta)^T \in \mathbb{R}^6$ denote the generalized coordinates where $\xi = (x, y, z)^T \in \mathbb{R}^3$ denotes the translation coordinates relative to the inertial frame $\mathcal{I}$, and $\eta = (\phi, \theta, \psi)^T \in \mathbb{R}^3$ describes the vehicle orientation

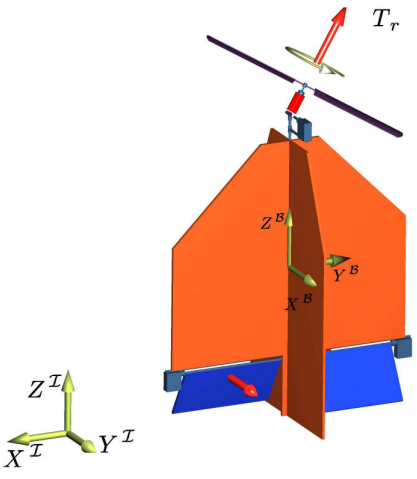

Fig. 2. Tail-sitter Tiltrotor UAV.

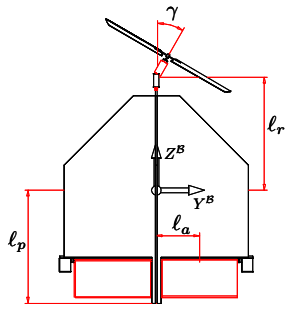

Fig. 3. Front view of the mini UAV.

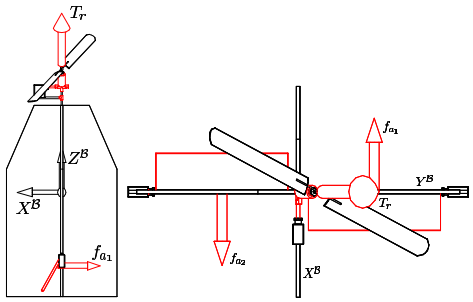

Fig. 4. Lateral and top views of the mini UAV.

expressed in the classical roll, pitch and yaw angles(Euler angles) (Goldstein et al. [1983]). The transformation matrix representing the orientation of this convertible UAV is given by $R^{\mathcal{B}\to\mathcal{I}}$.

$$R^{\mathcal{B}\to\mathcal{I}} = \begin{pmatrix} c_\theta c_\psi & -c_\theta s_\psi & s_\theta \\ c_\phi s_\psi + s_\phi s_\theta c_\psi & c_\phi c_\psi - s_\phi s_\theta s_\psi & -s_\phi c_\theta \\ s_\phi s_\psi - c_\phi s_\theta c_\psi & s_\phi c_\psi + c_\phi s_\theta s_\psi & c_\phi c_\theta \end{pmatrix}$$

where $s_a = sin(a)$, $c_a = cos(a)$. In this system the order of the rotations is considered as roll, pitch and yaw (ϕ, θ, ψ) (Stengel [2004]). For the roll motion, it is used an auxiliary rotation matrix $R^{\mathcal{R}\to\mathcal{B}}$. This rotation matrix results of the tilting motion about $i_x^{\mathcal{R}}$ axis and is given by

$$R^{\mathcal{R}\to\mathcal{B}} = \begin{pmatrix} 1 & 0 & 0 \\ 0 & c_\gamma & s_\gamma \\ 0 & -s_\gamma & c_\gamma \end{pmatrix}$$

where γ is the tilting angle and is related to the roll angle.

The Newton-Euler formulation provides the overall equations of motion of a rigid body which are given by the following vectorial expressions

$$\bar{m}\dot{v}^{\mathcal{B}} + \Omega \times \bar{m}v^{\mathcal{B}} = F^{\mathcal{B}} \quad (1)$$

$$\mathbf{I}\dot{\Omega} + \Omega \times \mathbf{I}\Omega = \Gamma^{\mathcal{B}} \quad (2)$$

where $F^{\mathcal{B}} \in \mathbb{R}^3$ and $\Gamma^{\mathcal{B}} \in \mathbb{R}^3$ are, respectively, the total force and torque applied to the center of gravity of the aircraft (CG), $\bar{m} = diag(m) \in \mathbb{R}^{3\times3}$, $m \in \mathbb{R}$ denotes the mass of the vehicle, $\Omega = (p, q, r)^T \in \mathbb{R}^3$ is the angular velocity of the vehicle from the center of mass, $v^{\mathcal{B}} = (u, v, w)^T \in \mathbb{R}^3$ is the translational velocity of the center of mass of the vehicle, $\mathbf{I} \in \mathbb{R}^{3\times3}$ contains the moments of inertia of the aircraft.

Translational motion The components of the thrust vector T are related to the angle γ, which denotes the tilt of the rotor. The vector thrust in terms of the body frame is described by

$$T^{\mathcal{B}} = R^{\mathcal{R}\to\mathcal{B}} T^{\gamma}$$

where $T^{\gamma} = (0, 0, T_r)^T \in \mathbb{R}^3$ is thrust vector of the rotor.

The translation motion relative to the body frame of the UAV is described by the following vectorial equation

$$\bar{m}\dot{v}^{\mathcal{B}} + \Omega \times \bar{m} v^{\mathcal{B}} = R^{\mathcal{I}\to\mathcal{B}} m G^{\mathcal{I}} + T^{\mathcal{B}} \tag{3}$$

where $G^{\mathcal{I}} \in \mathbb{R}^3$, $G^{\mathcal{I}} = (0, 0, -g)$ is the gravity vector.

The translation dynamics relative to the inertial frame is provided by the following expression

$$\begin{array}{rcl} \dot{\xi} & = & v^{\mathcal{I}} \\ m\dot{v}^{\mathcal{I}} & = & mG^{\mathcal{I}} + R^{\mathcal{B}\to\mathcal{I}} T^{\mathcal{B}} \end{array} \tag{4}$$

then

$$\begin{array}{rcl} \ddot{x} & = & T_r c_\gamma s_\theta - T_r s_\gamma c_\theta s_\psi \\ \ddot{y} & = & T_r s_\gamma c_\phi c_\psi - T_r s_\gamma s_\phi s_\theta s_\psi - T_r c_\gamma s_\phi c_\theta \\ \ddot{z} & = & T_r s_\gamma s_\phi c_\psi + T_r s_\gamma c_\phi s_\theta s_\psi + T_r c_\gamma c_\phi c_\theta - mg \end{array} \tag{5}$$

Rotational motion The RHS terms of (2) correspond to the applied torques on the rigid body, these torques are the following

Actuator torque The torque provided by the actuators is described by the following vectorial expression

$$\overrightarrow{\Gamma}_c = \overrightarrow{\ell} \times F \tag{6}$$

then

$$\Gamma_c = \begin{pmatrix} -\ell_r T_r s_\gamma \\ \ell_p (f_{a1} - f_{a2}) \\ \ell_a (f_{a1} + f_{a2}) \end{pmatrix}$$

where f_{a1} and f_{a2} represent the aileron lift forces of the vehicle.

Gyroscope torque The gyroscope torque caused by the tilting rotor is given by the following vectorial expression

$$\overrightarrow{\Gamma}_g = -I_r (\Omega \times \omega_r) \tag{7}$$

then

$$\Gamma_g = \begin{pmatrix} r w_r s_\gamma - q w_r c_\gamma \\ p w_r c_\gamma \\ -p w_r s_\gamma \end{pmatrix}$$

where I_r is the inertia moment of the propeller and w_r denotes the angular velocity of the rotor.

Weight torque The torque provided by the pendular mass is described by the following vectorial expression

$$\overrightarrow{\Gamma}_w = \overrightarrow{\ell_r} \times R^{\mathcal{I}\to\mathcal{B}} m G^{\mathcal{I}} \tag{8}$$

then

$$\Gamma_w = \begin{pmatrix} -mg\ell_r (c_\psi s_\phi + c_\phi s_\theta s_\psi) \\ -mg\ell_r (c_\phi s_\theta c_\psi - s_\phi s_\psi) \\ 0 \end{pmatrix}$$

Then, The total external torque in the body frame is written by the following expression

$$\Gamma^{\mathcal{B}} = \Gamma_c + \Gamma_g + \Gamma_w = \begin{pmatrix} \tau_M \\ \tau_L \\ \tau_N \end{pmatrix}$$

Therefore, the rotational dynamics in terms of the generalized coordinates is given by

$$\ddot{\eta} = (\mathbf{I} W_n)^{-1} (-\mathbf{I}\dot{W}_n \dot{\eta} - \Omega \times \mathbf{I}\Omega + \Gamma^{\mathcal{B}}) \tag{9}$$

where $W_n \in \mathbb{R}^3$ is a non-orthonormal transformation and Ω is the result of the projection of the vector $\dot{\eta}$ generated in each rotation.

The equation (9) can be rewritten as

$$\begin{array}{rcl} \ddot{\phi} & = & \dfrac{1}{c_\theta c_\psi}(s_\theta c_\psi \dot{\phi}\dot{\theta} + c_\theta s_\psi \dot{\phi}\dot{\psi} - c_\psi \dot{\theta}\dot{\psi} - s_\psi \ddot{\theta}) \\ & & + \dfrac{1}{I_x c_\theta c_\psi}[-qr(I_z - I_y) + \tau_M] \\ \ddot{\theta} & = & \dfrac{1}{c_\psi}(-s_\theta s_\psi \dot{\phi}\dot{\theta} + c_\theta c_\psi \dot{\phi}\dot{\psi} + s_\psi \dot{\theta}\dot{\psi} + c_\theta s_\psi \ddot{\phi}) \\ & & + \dfrac{1}{I_y c_\psi}[-pr(I_x - I_z) + \tau_L] \\ \ddot{\psi} & = & -c_\theta \dot{\phi}\dot{\theta} - s_\theta \ddot{\phi} + \dfrac{1}{I_z}[-pq(I_y - I_x) + \tau_N] \end{array} \tag{10}$$

with

$$\begin{array}{l} \tau_M = u_\phi + (q w_r c_\gamma - r w_r s_\gamma) - mg\ell_r (c_\psi s_\phi + c_\phi s_\theta s_\psi) \\ \tau_L = u_\theta - p w_r c_\gamma - mg\ell_r (c_\phi s_\theta c_\psi - s_\phi s_\psi) \\ \tau_N = u_\psi + p w_r s_\gamma \end{array}$$

where $u_\phi = -\ell_r T_r s_\gamma$, $u_\theta = \ell_p (f_{a1} - f_{a2})$ and $u_\psi = \ell_a (f_{a1} + f_{a2})$.

2.3 Reduced model

For purposes of control analysis, the full nonlinear 6-DOF model (4) and (9) is reduced by introducing the following assumptions and facts:

A1. The magnitude of the drag force is smaller than the magnitude of the lift and thrust forces.

A2. The lift force of the wing is neglected, due to the combination of the symmetric aerofoil of the wing and the direction of the air flow generated by the propeller which coincides with the zero-lift line of the wing.

A3. The unique aerodynamic force is generated by the deflexion of the control surfaces.

A4. The gyroscope torque generated by the tilt-propeller during the roll control is neglected.

A5. The inertial tensor matrix $\mathbf{I}$ and the vehicle mass m are normalized.

Considering the previous assumptions and facts the full nonlinear 6-DOF system (4) and (9) is partitioned into three sets of equations: lateral, longitudinal and axial subsystems.

Lateral subsystem This set of equations with ($\theta = 0$, $\psi = 0$) results of regulating the roll angle ϕ, and is given by

$$\begin{array}{l} \ddot{y} = -T_r \sin(\phi - \gamma) \\ \ddot{z} = T_r \cos(\phi - \gamma) - mg \\ \ddot{\phi} = u_\phi - mg\ell_r \sin(\phi) \end{array} \tag{11}$$

Longitudinal subsystem The longitudinal subsystem is the result of controlling the pitch angle θ with ($\phi = 0$, $\psi = 0$, $\gamma = 0$) and is given by

$$\begin{aligned} \ddot{x} &= T_r \sin(\theta) \\ \ddot{z} &= T_r \cos(\theta) - mg \\ \ddot{\theta} &= u_\theta - mg\ell_r \sin(\theta) \end{aligned} \tag{12}$$

Axial subsystem In this subsystem, the set of equations that results of controlling the yaw angle ψ with ($\phi = 0$, $\theta = 0$, $\gamma = 0$) is described by

$$\ddot{\psi} = u_\psi \tag{13}$$

3. CONTROLLER DESIGN

This section presents the control strategy to stabilize the T-Plane UAV in hovering flight. This controller is based on separated saturation functions (A.R. Teel [1992]).

For simplicity, we develop a control algorithm for the lateral, longitudinal and axial subsystems which lead to the control strategy for the full nonlinear 6-DOF system.

Analyzing the longitudinal subsystem (12), we propose a control input to stabilize the vertical position. This control input is described by

$$T_r = \frac{(r + mg)}{\cos(\theta)} \tag{14}$$

where

$$r = -k_{z1}\dot{z} - k_{z2}(z - z_d) \tag{15}$$

$m = 1$, z_d is desired altitude and k_{z1}, k_{z2} are positive constants.

Substituting (14) and (15) into (12), and considering that $z \to z_d$, $\dot{z} \to 0$ and $r \to 0$ as $t \to \infty$, we get the following reduced subsystem

$$\begin{aligned} \ddot{x} &= g \tan(\theta) \\ \ddot{\theta} &= u_\theta - g\ell_r \sin(\theta). \end{aligned} \tag{16}$$

Assuming that $\tan(\theta) \approx \theta$ and $\sin(\theta) \approx \theta$, the equations (16) are reduced to

$$\begin{aligned} \ddot{x} &= g\theta \\ \ddot{\theta} &= u_\theta - g\ell_r\theta \end{aligned} \tag{17}$$

which can be rewritten as

$$\begin{cases} \dot{x}_1 = x_2 \\ \dot{x}_2 = g\theta_1 \\ \dot{\theta}_1 = \theta_2 \\ \dot{\theta}_2 = u_\theta - g\ell_r\theta_1 \end{cases} \tag{18}$$

Now, we propose the following control input

$$u_\theta = g\ell_r\theta_1 - \sigma_{b_4}(k_4\theta_2) - \xi_1 \tag{19}$$

where $\sigma_\eta(s)$ is a ram-shaped saturation function which satisfies $\mid \sigma_\eta(s) \mid \leq \eta$ for some constant $\eta > 0$ and ξ_1 is a bounded function $\mid \xi_1 \mid \leq b_{\xi_1} > 0$ which will be defined later.

Substituting (19) into (18), we have

$$\dot{\theta}_2 = -\sigma_{b_4}(k_4\theta_2) - \xi_1 \tag{20}$$

Consider the following positive definite function

$$V_4 = \frac{1}{2}\theta_2^2 \tag{21}$$

then

$$\dot{V}_4 = -\theta_2(\sigma_{b_4}(k_4\theta_2) + \xi_1) \tag{22}$$

we assume that $b_4 > b_{\xi_1}$. Then $\mid k_4\theta_2 \mid > b_{\xi_1}$ implies $\dot{V}_4 < 0$. There exists a time t_1 such that

$$\mid \theta_2 \mid \leq \frac{b_{\xi_1}}{k_4} \qquad \forall t > t_1 \tag{23}$$

This implies that

$$\dot{\theta}_2 = -k_4\theta_2 - \xi_1 \tag{24}$$

We propose ξ_1 as

$$\xi_1 = \sigma_{b_3}(k_3\theta_1) + \xi_2 \tag{25}$$

where $\mid \xi_2 \mid \leq b_{\xi_2}$ for some positive constant b_{ξ_2}.

Consider

$$z_3 = k_4\theta_1 + \theta_2 \tag{26}$$

then

$$\dot{z}_3 = -\sigma_{b_3}(k_3\theta_1) - \xi_2 \tag{27}$$

Consider the following positive definite function

$$V_3 = \frac{1}{2}z_3^2 \tag{28}$$

then

$$\dot{V}_3 = -(k_4\theta_1 + \theta_2)(\sigma_{b_3}(k_3\theta_1) + \xi_2) \tag{29}$$

We assume that $b_3 > b_{\xi_2}$. Note that when $\mid \theta_1 \mid > \frac{b_{\xi_1}}{k_4^2}$ implies

$$k_4 \mid \theta_1 \mid > \mid \theta_2 \mid \Rightarrow \operatorname{sgn}(k_4\theta_1 + \theta_2) = \operatorname{sgn}(\theta_1) \tag{30}$$

on the other hand, if $\mid \theta_1 \mid > \frac{b_{\xi_2}}{k_3}$ implies

$$\mid \sigma_{b_3}(k_3\theta_1) \mid > \mid \xi_2 \mid \Rightarrow \operatorname{sgn}(\sigma_{b_3}(k_3\theta_1) + \xi_2) = \operatorname{sgn}(\theta_1) \tag{31}$$

then for $\mid \theta_1 \mid > \frac{b_{\xi_2}}{k_3} > \frac{b_{\xi_1}}{k_4^2}$ implies $\dot{V}_3 < 0$. There exists a time $t_2 > t_1$ such that

$$\mid \theta_1 \mid \leq \frac{b_{\xi_2}}{k_3} \qquad \forall t > t_2 \tag{32}$$

This implies that

$$\dot{\theta}_2 = -k_4\theta_2 - k_3\theta_1 - \xi_2 \qquad \forall t > t_2 \tag{33}$$

We propose ξ_2 as

$$\xi_2 = \sigma_{b_2}(k_2x_2) + \xi_3 \tag{34}$$

where $\mid \xi_3 \mid \leq b_{\xi_3}$ for some positive constant b_{ξ_3}.

Consider

$$z_2 = \frac{k_3}{g}x_2 + z_3 \tag{35}$$

then

$$\dot{z}_2 = -\sigma_{b_2}(k_2x_2) - \xi_3 \tag{36}$$

Consider the following positive definite function

$$V_2 = \frac{1}{2}z_2^2 \tag{37}$$

then

$$\dot{V}_2 = -\left(\frac{k_3}{g}x_2 + k_4\theta_1 + \theta_2\right)(\sigma_{b_2}(k_2x_2) + \xi_3) \tag{38}$$

We assume that $b_2 > b_{\xi_3}$. Similarly as above procedure for $\mid x_2 \mid > \frac{b_{\xi_3}}{k_2} > \frac{k_4 g b_{\xi_2}}{k_3^2} + \frac{g b_{\xi_1}}{k_3 k_4}$ implies $\dot{V}_2 < 0$. There exists a time $t_3 > t_2$ such that

$$| x_2 | \leq \frac{b_{\xi_3}}{k_2} \qquad \forall t > t_3 \tag{39}$$

This implies that

$$\dot{\theta}_2 = -k_4\theta_2 - k_3\theta_1 - k_2x_2 - \xi_3 \qquad \forall t > t_3 \tag{40}$$

We propose ξ_3 as

$$\xi_3 = \sigma_{b_1}(k_1x_1) \tag{41}$$

Consider

$$z_1 = k_2x_1 + z_2 \tag{42}$$

then

$$\dot{z}_1 = -\sigma_{b_1}(k_1x_1) \tag{43}$$

Consider the following positive definite function

$$V_1 = \frac{1}{2}z_1^2 \tag{44}$$

then

$$\dot{V}_1 = -\left(k_2x_1 + \frac{k_3}{g}x_2 + k_4\theta_1 + \theta_2\right)(\sigma_{b_1}(k_1x_1)) \tag{45}$$

We assume that $b_1 > 0$. For $| x_1 | > \frac{k_3b_{\xi_3}}{gk_2^2} + \frac{k_4b_{\xi_2}}{k_2k_3} + \frac{b_{\xi_1}}{k_2k_4}$ implies $\dot{V}_1 < 0$. There exists a time $t_4 > t_3$ such that

$$| x_1 | \leq \frac{k_3b_{\xi_3}}{gk_2^2} + \frac{k_4b_{\xi_2}}{k_2k_3} + \frac{b_{\xi_1}}{k_2k_4} \qquad \forall t > t_4 \tag{46}$$

then if

$$\frac{k_3b_{\xi_3}}{gk_2^2} + \frac{k_4b_{\xi_2}}{k_2k_3} + \frac{b_{\xi_1}}{k_2k_4} \leq \frac{b_1}{k_1} \tag{47}$$

that implies that

$$u_\theta = g\ell_r\theta_1 - k_4\theta_2 - k_3\theta_1 - k_2x_2 - k_1x_1 \qquad \forall t > t_4 \tag{48}$$

The system (18) reduces to

$$\begin{pmatrix} \dot{x_1} \\ \dot{x_2} \\ \dot{\theta_1} \\ \dot{\theta_2} \end{pmatrix} = \begin{pmatrix} 0 & 1 & 0 & 0 \\ 0 & 0 & g & 0 \\ 0 & 0 & 0 & 1 \\ -k_1 & -k_2 & -(g\ell_r + k_3) & -k_4 \end{pmatrix} \begin{pmatrix} x_1 \\ x_2 \\ \theta_1 \\ \theta_2 \end{pmatrix}$$

Choosing k_1, k_2, k_3 and k_4 such that the previous matrix is Hurwitz. This implies that the state vector $(x_1, x_2, \theta_1, \theta_2)^T$ is stable.

The control input u_θ is given by (19), (25), (34) and (41)

$$u_\theta = g\ell_r\theta_1 - \sigma_{b_4}(k_4\theta_2) - \sigma_{b_3}(k_3\theta_1) - \sigma_{b_2}(k_2x_2) - \sigma_{b_1}(k_1x_1) \tag{49}$$

In order to stabilize the lateral subsystem (11), we assume that $T_r \approx g$. Also we consider $\sin(\phi) \approx \phi$ and $\sin(\gamma) \approx \gamma$ since ϕ and γ are relatively small.

$$\begin{aligned} \ddot{y} &= -g\phi \\ \ddot{\phi} &= u_\phi - g\ell_r\phi \end{aligned} \tag{50}$$

To obtain the control input that renders the previous dynamics (50) to the origin, we recall the control methodology employed to stabilize the longitudinal dynamics (12). Thus, the control input is given by

$$u_\phi = g\ell_r\phi_1 - \sigma_{b_4}(k_4\phi_2) - \sigma_{b_3}(k_3\phi_1) - \sigma_{b_2}(k_2y_2) - \sigma_{b_1}(k_1y_1) \tag{51}$$

On the other hand, analyzing the axial subsystem (13), we propose a control input which is described by

$$u_\psi = -k_{\psi 1}\dot{\psi} - k_{\psi 2}\psi \tag{52}$$

where $k_{\psi 1}$ and $k_{\psi 2}$ are positive constants.

Substituting (52) into (13), we have

$$\ddot{\psi} = -k_{\psi 1}\dot{\psi} - k_{\psi 2}\psi \tag{53}$$

therefore $\dot{\psi} \to 0$ and $\psi \to 0$ as $t \to \infty$.

It is important to point out that experimentally the proposed nonlinear control laws (49) and (51) perform well even in presence of significant disturbances.

4. SIMULATION RESULTS

In this section, we present the simulation results of the the full nonlinear 6-DOF model in hovering flight. Simulations show the performance using a controller based on separated saturation functions to stabilize the orientation and position of the T-Plane UAV. The parameters used for the simulations are $k_{z1} = 5$, $k_{z2} = 6$, $k_{\psi 1} = 4$, $k_{\psi 2} = 4$, $k_1 = 0.16$, $k_2 = 1.06$, $k_3 = 3.51$, and $k_4 = 2.60$.

The initial conditions for the simulations are $x(0) = 0.1$, $y(0) = 0.1$, $z(0) = 0.1$, $\phi(0) = \frac{\pi}{15}$, $\theta(0) = \frac{\pi}{15}$, $\psi(0) = \frac{\pi}{15}$ and the desired altitude is $z_d = 2$m. The position response of the closed loop system is depicted in Fig. 5a. We can observe that the vehicle is stable during the vertical flight. The behavior of the attitude using the nonlinear controller based on separated saturation functions is illustrated in Fig. 5b. The Fig. 6 shows the control inputs of the T-Plane UAV using the nonlinear controller.

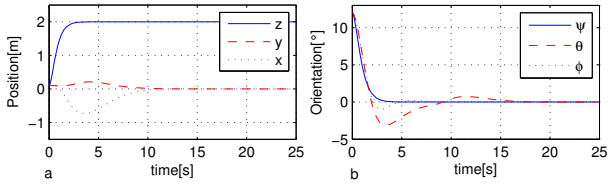

Fig. 5. Position and attitude of the T-Plane.

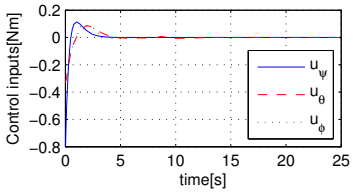

Fig. 6. Control inputs of the T-Plane.

5. EXPERIMENTAL RESULTS

In this section we present the detailed experimental platform (T-Plane UAV) built at the Heudiasyc Laboratory. In addition, the experimental results are shown to validate the nonlinear controller in the T-Plane UAV.

5.1 Experimental platform

The main frame of the vehicle is made of carbon fiber and flat foam sheet. The aircraft is driven by one brushless

motor. The vehicle is operated by a low-cost embedded microcontroller and a homemade inertial measurement unit(IMU). The microcontroller is a Rabbit RCM3400 microcontroller with a 512 Kb flash memory, a 29.4 MHz processor and a 12 bit Analog-Digital converter. This microcontroller is used to store the control algorithm implemented in dynamic C environment. The IMU has a dual-axis accelerometer sensor (accelerometer ADXL203) and three angular rate sensors (gyroscope ADXRS150) arranged in orthogonal position. The IMU provides two angular position (ϕ, θ) and three angular rates $(\dot{\phi}, \dot{\theta}, \dot{\psi})$.

The Analog-Digital converter receives the IMU signals, then the microcontroller processes that information and sends the control inputs (Pulse-width modulation signals) to the actuators.

5.2 Experimental test

This section shows the experimental results in hovering flight of the T-Plane UAV. The Fig. 7 shows the T-Plane UAV hovering autonomously. As can be seen from Fig. 8, 9 and 10 the proposed controller stabilizes the aircraft even in presence of disturbances.

Fig. 7. The T-Plane UAV hovering autonomously.

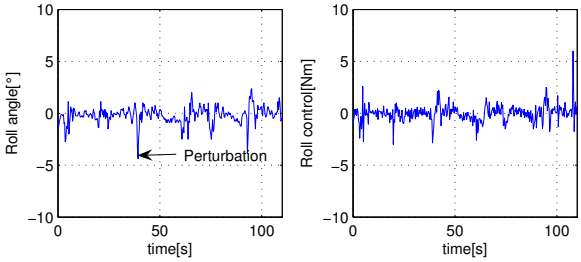

Fig. 8. Roll angle and roll control.

6. CONCLUDING REMARKS AND PERSPECTIVES

We have presented in detail the dynamic model of a tilting single-rotor vehicle (T-Plane UAV). We have contributed with a single-rotor configuration that shows a robust behavior with respect to external perturbation. In terms of control, we have used an on-board saturation-based algorithm that provides a stabilized hover flight. The challenge arising from this kind of vehicles (CUAVs) is to provide a control algorithm for the whole flight envelope (both modalities), as well as a reliable position sensor (GPS, optic flow).

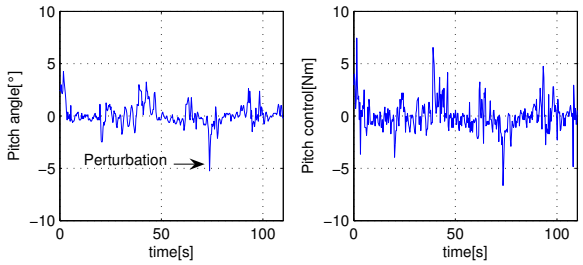

Fig. 9. Pitch angle and pitch control.

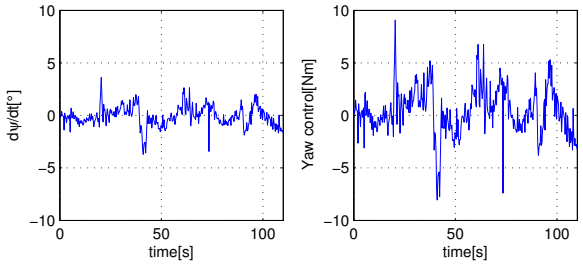

Fig. 10. Yaw angular rate and yaw control.

REFERENCES

P. Castillo, R. Lozano, and A. Dzul. Modelling and control of miniflying machines. *Springer-Verlag*, London, July 2005.

B. D. Etkin. Dynamics of flight. *John Wiley and Sons*, Inc., New York, 1991.

I. Fantoni, and R. Lozano. Nonlinear control of underactuated mechanical systems. *Springer-verlag*, London, 2002.

H. Goldstein, C.P. Poole and J.L Safko. Classical Mechanics. *Addison Wesley Series in Physics, Adison-Wesley*, U.S.A., second edition, 1983.

H. Khalil. Nonlinear Systems. *Prentice Hall*, New York, 1995.

A. Sanchez, P. Castillo, J. Escareño, H. Romero and R. Lozano. Simple real-time control strategy to stabilize the PVTOL aircraft using bounded inputs. *European Control Conference*, Kos, Greece,2-5 July, 2007.

R. F. Stengel. Flight Dynamics. *Princeton University Press*, U.S.A., 2004.

H. Stone. Aerodynamic modelling of a wing-in-slipstream tailsitter UAV. *Biennial International Powered Lift Conference*, Williamsburg, Virginia, Nov. 5-7, 2002.

A. R. Teel. Global stabilization and restricted tracking for multiple integrators with bounded controls. *Systems and Control Letters*, 1992.